Geochemistry, Geophysics, Geosystems®

RESEARCH ARTICLE
10.1029/2025GC012516

Geodynamic Controls on Mantle Differentiation and Preservation of Long-Term Geochemical Heterogeneity: Focus on the Primitive Undegassed Mantle

Nicolas Récalde[1], J. Huw Davies[1], James Panton[1,2], Don Porcelli[3], and Morten Andersen[1]

[1]School of Earth and Environmental Sciences, Cardiff University, Cardiff, UK, [2]Now at Institute of Geophysics and Meteorology, University of Cologne, Köln, Germany, [3]Department of Earth Sciences, University of Oxford, Oxford, UK

Key Points:

- Thermal evolution is a significant control of the mantle processing history and of the type of material that can melt
- Preservation of heterogeneity is strongly dependent on processing history which converges within present-day estimates for most simulations
- While efficient mantle mixing favors sampling of heterogeneities it also promotes cooling which can contribute to their preservation

Supporting Information:

Supporting Information may be found in the online version of this article.

Correspondence to:

N. Récalde,
recalden@cardiff.ac.uk

Citation:

Récalde, N., Davies, J. H., Panton, J., Porcelli, D., & Andersen, M. (2026). Geodynamic controls on mantle differentiation and preservation of long-term geochemical heterogeneity: Focus on the primitive undegassed mantle. *Geochemistry, Geophysics, Geosystems*, *27*, e2025GC012516. https://doi.org/10.1029/2025GC012516

Received 17 JUN 2025
Accepted 2 MAR 2026

Author Contributions:

Conceptualization: Nicolas Récalde, J. Huw Davies
Data curation: Nicolas Récalde, J. Huw Davies, James Panton
Formal analysis: Nicolas Récalde
Funding acquisition: J. Huw Davies
Investigation: Nicolas Récalde
Methodology: Nicolas Récalde
Project administration: Nicolas Récalde, J. Huw Davies
Resources: J. Huw Davies

Abstract The compositional evolution of the Earth's mantle is the result of mantle differentiation and thermal evolution. Partial melting of mantle materials produces geochemical heterogeneities, allows for degassing and depends on the thermal state of the mantle, itself governed by convection. Helium and argon constraints suggest that the Earth's mantle is not fully degassed, implying the preservation of long-term heterogeneities, including the primitive undegassed mantle. While previous research has shown that the preservation of old heterogeneities can be improved by increasing the material's density or viscosity, the role of mantle dynamics in controlling mantle differentiation remains unclear. Therefore, using 3D spherical mantle convection simulations tracking bulk composition and degassing, we investigate the influence of mantle viscosity, heat-producing elements (HPEs) enrichment and initial temperature on mantle differentiation. The resulting preservation of primitive undegassed material is systematically analyzed. Results show that thermal evolution (i.e., the cooling history of the mantle) is the main control of the processing history. The ability of the mantle to release its heat, also determined by shallow conditions, governs the processing rates and the types of material processed within melting zones. Models testing the influence of HPEs concentration and initial temperature all reach Earth's current processing rate estimates but primitive undegassed material preservation varies between $\approx 1\% - 30\%$ after 5 Gyr. Therefore, the processing history is crucial when studying preservation of long-term heterogeneities. The dispersal of the unsampled primitive material by convection allows its temperature to converge to that of the average mantle, promoting its preservation.

Plain Language Summary Partial melting of mantle materials allows for degassing and creates compositional heterogeneities that can be preserved for several billion years as suggested by geochemical observations. Helium and argon data suggest that heterogeneities, potentially nearly as old as the age of the Earth, undegassed, are preserved within the planet's interior. Previous works have shown that increasing the viscosity or density of mantle materials can help maintaining them from melting and degassing. However, the role of mantle convection in controlling the amount of material processed in melting zones through time (i.e., the processing history) is unclear. Therefore, the influence of fundamental convection parameters (e.g., viscosity, radiogenic heat input) on the processing history are investigated using 3D spherical simulations. The resulting preservation of primitive undegassed material is systematically analyzed. Results show that the processing history relates to the thermal evolution of the mantle and that different types of material are processed depending on surface velocities and shallow temperatures. A preservation mechanism is the dispersal of primitive material by convection, allowing the material's temperature to converge to that of the average mantle. Results show that some geodynamical contexts and processing histories are more favorable to the preservation of material than others.

1. Introduction

Mantle dynamics controls both thermal and compositional evolution of the mantle. Thus, it is key to better understand the variety of geochemical heterogeneities in the context of mantle dynamics. Mantle derived samples, Mid-Oceanic Ridge Basalts (MORBs) and Oceanic Island Basalts (OIBs), reveal the presence of these heterogeneities in trace element abundances and radiogenic isotope ratios (e.g., Sr, Nd, Hf, Pb, He, Ar, Xe, Hofmann, 1997, 2007). While geochemical tracers are used to characterize mantle sources (Stracke et al., 2005), helium and argon systems provide major constraints on mantle evolution. First because of their geochemical affinities that makes them ideal tracers, second because their radiogenic isotopes are daughters of the main Heat-

Software: Nicolas Récalde, J. Huw Davies, James Panton
Supervision: J. Huw Davies, James Panton, Don Porcelli, Morten Andersen
Validation: Nicolas Récalde, J. Huw Davies
Visualization: Nicolas Récalde
Writing – original draft: Nicolas Récalde
Writing – review & editing: Nicolas Récalde, J. Huw Davies, James Panton, Don Porcelli, Morten Andersen

Producing Elements (HPEs) of the mantle (^{3}He and ^{36}Ar are primordial while ^{4}He is produced by decay of ^{235,238}U and ^{232}Th and ^{40}Ar by decay of ^{40}K). Measurements of the ^{3}He/^{4}He ratio and ^{40}Ar/^{36}Ar ratio in mantle derived samples reveal that OIBs display a more primitive (or less radiogenic) signature than MORBs (Hilton & Porcelli, 2003; Kurz, Jenkins, & Hart, 1982; Kurz, Jenkins, Schilling, & Hart, 1982; Porcelli & Wasserburg, 1995). Additionally, the fact that both OIBs and MORBs ^{3}He/^{4}He ratios are higher than atmospheric (He is subject to atmospheric escape, MacDonald, 1963) implies significant degassing of primordial He (Hilton & Porcelli, 2003). Regarding Ar, about half of the ^{40}Ar budget is seemingly still trapped in the solid Earth (Albarède & van der Hilst, 2002; Allègre & Turcotte, 1986). Noble gases (He, Ar) therefore imply incomplete degassing of the mantle, and require the preservation of undegassed (or not fully degassed) material (Albarède & van der Hilst, 2002; Farley et al., 1992; Jackson et al., 2010; Mukhopadhyay & Parai, 2019). Further radiogenic systems (short-lived systems), for example ^{129}I-^{129}Xe (Mukhopadhyay & Parai, 2019) and ^{146}Sm-^{142}Nd (Bennett et al., 2007) also require long-term preservation of heterogeneities. A question is how is this achieved within the convecting mantle?

The primitive mantle, whether considered as similar to the Bulk Silicate Earth (BSE) (Stracke, 2025) or as the least evolved/processed material (Mukhopadhyay & Parai, 2019), is a candidate to host the primordial noble gases (e.g., ^{3}He, ^{36}Ar) and part of the "missing" ^{40}Ar. The preservation of the primitive mantle and other long-term heterogeneities is however difficult to reconcile with the geophysical understanding of the mantle. Indeed, seismic tomography images refute layered mantle convection in favor of whole mantle convection (Albarède & van der Hilst, 2002; van der Hilst et al., 1997), although mass transfers between the lower and the upper mantle remain poorly constrained (French & Romanowicz, 2015; Fukao & Obayashi, 2013; Kárason & Van Der Hilst, 2000). For that reason, the question of the survival of long-term heterogeneities has been studied with geodynamic models. The effects of mantle convection itself are destructive to heterogeneities, as mixing and stirring reduces the length scale of these heterogeneities (Ferrachat & Ricard, 1998; Hoffman & McKenzie, 1985; Kellogg & Turcotte, 1987; van Keken et al., 2002), ultimately allowing diffusive equilibration if reduced to the meter scale. Assumptions on the physical properties of heterogeneities have been made to counter these effects of mantle convection. For example, increased material viscosity provides good resistance against mixing and stirring and promotes preservation (Ballmer et al., 2017; Becker et al., 1999; Gülcher et al., 2021). Moreover, multiple geodynamic studies focus on generating basal mantle structures that are intrinsically denser than the ambient mantle. They can be constituted of dense primordial material that is inherited from interactions between the solid mantle and the solidifying basal magma ocean (Labrosse et al., 2007), or from the moon-forming impact (Yuan et al., 2023). They could also be constituted of dense recycled oceanic crust (Christensen & Hofmann, 1994; Panton et al., 2023) or a mixture of recycled and primordial material (Gülcher et al., 2021; Jones et al., 2021). These basal mantle structures are also called thermo-chemical piles. The intrinsic density excess confers strong negative buoyancy to the material, promoting its preservation by convective isolation in the lowermost mantle (Guerrero et al., 2023; Heyn et al., 2018; M. Huang et al., 2022; Jones et al., 2021; Y. Li et al., 2022; Panton et al., 2023; Tucker et al., 2022; Yuan et al., 2023). These studies are also motivated by the ubiquitous observation of Large Low Shear Velocity Provinces in seismic tomography models (e.g., French & Romanowicz, 2014; Ritsema et al., 2011; Koelemeijer et al., 2016). The observed structures are associated with mantle plumes and intra-plate volcanism (French & Romanowicz, 2015), making them candidates to hold the material(s) responsible for more primitive and less degassed signatures found in OIBs.

Another process against the preservation of heterogeneity that is not mentioned as often, yet fundamental, is mantle differentiation. It refers to the melting process that generates new heterogeneities, destroying older ones, and allowing degassing. J. Huang and Davies (2007a, 2007b) highlighted the importance that the amount of processing has on the preservation of heterogeneities. Estimates for Earth's recent processing rate, that is the mass of mantle material that has had melt extracted during a period of time, are calculated using the area of oceanic crust of a given age, assuming a thickness, a density, and a fraction of partial melting. Processing rates are difficult to constrain and estimates vary between $4.10^{14}-3.10^{15}$ kg.yr^{-1} (Kellogg & Wasserburg, 1990; M. Li et al., 2016; Nakagawa & Tackley, 2012; Phipps Morgan, 1998; Stracke, 2025; Tackley, 2015). Previous geodynamic modeling studies focus on matching the Earth's mantle current convection vigor (by matching surface velocities $\simeq$5 cm.yr^{-1}, Müller et al., 2022) and current surface heat flux ($90-100$ mW.m^{-2}, $40-50$ *TW*, J. H. Davies & Davies, 2010; Jaupart et al., 2015; Sammon & McDonough, 2022) to reproduce the estimated mantle processing and melt production rate (J. Huang & Davies, 2007a; Jones et al., 2021; M. Li et al., 2016; Tucker et al., 2022). However, the result of these models is a rather constant processing rate throughout simulation time. Supposing

Table 1
Parameters Common to All Presented Simulations

Symbol	Parameter	Value	Unit
g	Gravitational acceleration	10	$m.s^{-2}$
T_S	Surface temperature	300	K
T_{CMB}	Core-Mantle Boundary temperature	3,000	K
ρ_0	Reference density	4,500	$kg.m^{-3}$
k	Thermal conductivity	4	$W.m^{-1}K^{-1}$
α	Thermal expansivity	2.5×10^{-5}	K^{-1}
C_P	Specific heat capacity	1,100	$J.kg^{-1}K^{-1}$
$\Delta\rho_{410}$	Density difference for 410 phase transition	230	$kg.m^{-3}$
$(\partial P/\partial T)_{410}$	Clapeyron Slope for 410 phase transition	1.5	$MPa.K^{-1}$
$\Delta\rho_{660}$	Density difference for 660 phase transition	380	$kg.m^{-3}$
$(\partial P/\partial T)_{660}$	Clapeyron Slope for 660 phase transition	-1	$MPa.K^{-1}$

that processing rates are mostly dependent on spreading rates, c.a. the vigor of convection, and that the latter is likely to have been higher earlier in Earth history, former studies present a lower bound to Earth processing history. Such studies thus potentially favor the preservation of heterogeneities within the mantle. We note that no matter what the processing history of the Earth is, it should reconcile with the atmospheric budget of ^{40}Ar (Allègre & Turcotte, 1986).

While the role of convective mixing (Coltice, 2005; Ferrachat & Ricard, 1998, 2001) and processing rates was shown to be primary for preserving long-term heterogeneities (J. Huang & Davies, 2007a, 2007b), the role of mantle dynamics (as the driver of thermal evolution) in controlling these processing rates remains unclear. So are the consequences of different processing histories (i.e., evolution of processing rates) on the preservation of primitive undegassed material. In this contribution, we thus investigate the influence of mantle dynamics on the processing history of the mantle, using 3D spherical mantle convection models in order to include accurate mixing, especially in the upper mantle (Ferrachat & Ricard, 1998). We explore a range of parameters such as the initial thermal state (secular heat), the convection vigor, the radiogenic heating rate and the viscosity structure, which are determinant to Earth thermal evolution. The aim is to understand how each parameter impacts the processing rates and the resulting preservation of geochemical heterogeneity, focusing on the primitive undegassed mantle. We investigate the ability of mantle dynamics to favor the sampling of certain heterogeneities, with the idea that a selective sampling promotes a relative preservation of other heterogeneities.

2. Materials and Methods

2.1. Geodynamic Model

The presented models use the three-dimensional spherical mantle convection code TERRA (Baumgardner, 1985; Bunge et al., 1997; D. R. Davies et al., 2013; van Heck et al., 2016). The governing equations for heat transfer, that is mass, momentum and energy conservation are solved under the Boussinesq approximation, assuming incompressibility. A regular icosahedron projected onto a sphere is used on each of the 65 radial layers (radial spacing of 45 km, Baumgardner & Frederickson, 1985; Yang, 1997). The grid is further discretized so that the average lateral spacing is ≈33 km at the Core Mantle Boundary (CMB) and ≈60 km at the surface ($mt = 128$). The boundary conditions are free-slip, iso-thermal and constant with a value of 3000 K and 300 K at the CMB and the surface, respectively. The dynamic effect of phase transitions at 410 km and 660 km depth is included in the presented simulations. Constant parameters are reported in Table 1.

2.2. Particles and Differentiation

Particles are used to track bulk composition and trace elements to simulate thermo-chemical convection. Bulk composition is bound to vary between 0 and 1, which can be viewed as a level of enrichment of basaltic components, where $C = 0$ is fully depleted (harzburgite) and $C = 1$ is fully enriched material (basalt). The average

mantle composition in our models is $C = 0.2$ (lherzolite). The bulk composition affects the density so that enriched material is 4% denser than fully depleted material in the upper mantle and 3% denser in the lower mantle. The "basalt barrier" effect, caused by the delayed transition to lower-mantle mineral phases of the cold subducted crust (Irifune & Ringwood, 1993), is modeled by making enriched composition 5% more buoyant between 660 and 750 km depth (Ono et al., 2001; G. F. Davies, 2008). We simulate melting in our simulations with a simple solidus that is dependent on both depth (z) and bulk composition (Panton et al., 2023; Price et al., 2019; van Heck et al., 2016), with the parametrization of Panton et al. (2022):

$$T_{solidus}(z, C) = T_{meltsurf} + zT_{meltslope} + (1 - C)T_{meltcomp} \quad (1)$$

with $T_{meltsurf} = 1200\ K$ corresponding to the melting temperature of a fully enriched material at the surface, $T_{meltslope} = 2.5\ \text{K.km}^{-1}$ the gradient of the solidus and $T_{meltcomp} = 500\ K$ the temperature difference between the solidi of fully depleted ($C = 0$) and fully enriched material ($C = 1$). This melting method does not affect the temperature field and thus conserves energy, meaning that the effects of latent heat and thermal advection caused by melt transport are neglected. This assumption could lead to underestimating the thermal cooling of a simulation, particularly one with intense magmatism or when modeling early Earth thermal evolution (Xie & Tackley, 2004).

In TERRA, melting happens at the particle level. After particles have been advected by the mantle flow, temperature is interpolated from the neighboring grid nodes to the tracers (van Heck et al., 2016). The melting domain is the region where melting is allowed, which is restricted to the uppermost 270 km of the mantle. When a particle's temperature is higher than its solidus, the particle is depleted so that the melting temperature for the new composition matches the particle's temperature. In other words, since the particle's temperature is not changed, the particle's composition and thus its solidus are adjusted so that the particle will no longer produce melt at the given pressure and temperature conditions (van Heck et al., 2016). Later on, if the particle is advected to a lower pressure domain, it could then undergo further melting and depletion. The degree of melting (F) is calculated as follows:

$$F = C_n - C_{n+1} \quad (2)$$

with C_n and C_{n+1} being the composition of the particle before and after melting, respectively. As a consequence, when a particle is fully depleted ($C = 0$), it cannot produce melt anymore. The amount of melt generated ($Melt$) for a particle is thus:

$$Melt = M_{particle} \times F \quad (3)$$

with $M_{particle}$ being the mass of the particle and F the degree of melting. The amount of melt ($Melt$), which equates to an amount of enrichment in basaltic components, is then redistributed to the uppermost particles within the same radial column. If a particle is already fully enriched but there is still melt to emplace, another particle within the same cell is enriched and so repeatedly until exhaustion of $Melt$. When all particles of the uppermost cell are fully enriched in basalt, the melt is emplaced in the particles of the immediately underlying cell. Thus, the depth of melt emplacement depends on the amount of $Melt$ and surface spreading rates. Sometimes, all of the particles above the melting particle are already filled in enriched component ($C = 1$), in which case the melt is emplaced in the producing particle, which very likely will melt again at the next time step. This limitation does not happen frequently and is negligible in most of our simulations (figure S1 in Supporting Information S1).

Regarding trace elements, the number of atoms (A_m) incorporated in the melt is computed as follows:

$$A_m = \frac{A_0}{F + (D(1 - F))} \quad (4)$$

with A_0 the number of atoms held by the melting particle, F the degree of melting and D the appropriate partition coefficient. For elements like Ar that are not only highly incompatible but also have a very low silicate melt

Table 2
Presented Simulations and Varying Parameters

Run name	η_{ref} (Pa.s)	Lithospheric viscosity factor	Initial mantle depletion *idpltd* (%)	Average initial temperature (*K*)
05_depltd	5.10^{21}	5	50	1,950
03_depltd	5.10^{21}	5	30	1,950
07_depltd	5.10^{21}	5	70	1,950
1_22_visc	1.10^{22}	5	50	1,950
3_22_visc	3.10^{22}	5	50	1,950
no_lid_visc	5.10^{21}	1	50	1,950
10_lid_visc	5.10^{21}	10	50	1,950
lT_init	5.10^{21}	5	50	1,565
hT_init	5.10^{21}	5	50	2,211

Note. Reference viscosity is the viscosity of the upper mantle.

solubility, 90% of the Ar atoms that are within the melt are taken out of the system and added to a virtual atmosphere.

2.3. Parameter Space and Initialization

Table 2 contains the suite of presented models and their differences. Models have a depth-dependent viscosity with a profile going from 1 to 30 times the reference viscosity as depth approaches the lower mantle at 660 km, and a drop when approaching the CMB to approximate the effect of the Thermal Boundary Layer (TBL) (Figure S2 in Supporting Information S1). At the surface, there is an increase in the viscosity to account for the lithosphere. The effect of the strength of the lithosphere (its viscosity) is tested with cases *no_lid_visc* and *10_lid_visc* as we expect it to scale the surface velocities (Table 2 and figure S2 in Supporting Information S1). Simulations start with a homogeneous bulk composition of $C = 0.2$. Each of the HPEs, that is ^{238,235}U, ^{232}Th, ^{40}K and other isotopes are homogeneously distributed between particles. The HPE content is calculated according to the BSE values of Arevalo et al. (2009) projected 4.5 Gyr ago. As the HPEs isotopes progressively decay into their respective daughter isotopes, the amount of heat they provide decreases. As the mantle differentiates and because of the overall incompatible nature of the HPEs, they are also concentrated in enriched material, which allows us to make the internal heating of our simulation time and spatially dependent (van Heck et al., 2016).

Before the start of the simulation, the mantle is depleted homogeneously of its HPEs so that

$$X_{Mantle} = (1 - idpltd) \times X_{BSE} \tag{5}$$

with X_{mantle} the amount of a given HPE within the convecting mantle at the start of the simulation, *idpltd* the initial depletion factor (Table 2) and X_{BSE} the amount of a given HPE for the BSE. We investigate this range since the initial HPE budget of the BSE is still debated and processes such as continental crust formation would deplete the mantle of its HPEs. Also, we want to investigate the influence of such variation since it is known that radioactive heating has a strong influence on mantle convection (Bercovici et al., 1989). The simulated mantle of models *03_depltd*, *05_depltd*, and *07_depltd* is initiated with 70%, 50% and 30% of the total amount of HPEs, respectively. The initial thermal state is obtained with a first simulation of purely thermal convection, with constant homogeneous radiogenic heating. Once steady-state has been reached (i.e., approximately no temporal variation of temperature, heat fluxes and surface velocities), the temperature, pressure and velocity fields are used to start the main simulation, where composition and isotopes (which will dictate radiogenic heating) are initialized. Different heating rates are applied in order to produce the three initial thermal states used as starting conditions of the presented runs, which we distinguish by their average temperature (volume average, Table 2). This preconditioning step is important to minimize the perturbation that the initial thermal state can produce on the dynamics of the system (first generation of upwellings and overturn) and the analyzed metrics (e.g., processing rates).

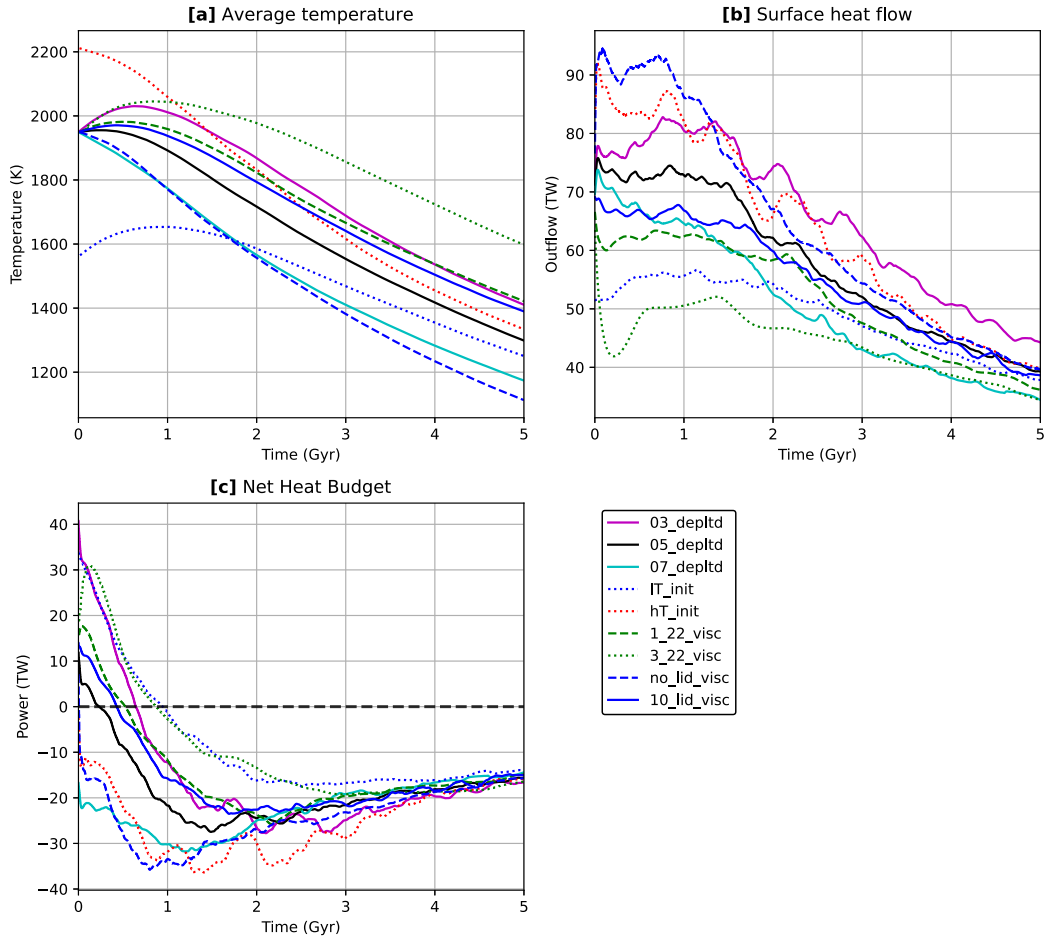

Figure 1. Average mantle temperature (volume average) (a), surface heat flux (b), and net heat budget (c) as a function of time for presented simulations. In panel (c), positive values mean that the mantle is heating up and negative values mean that it is cooling.

3. Results

3.1. Thermal Evolution and Mantle Differentiation

Presented models test the impact of various parameters that are key to the thermal evolution of the mantle. Amongst them, models *05_depltd*, *lT_init* and *hT_init* share the same dynamic parameters but they have different initial thermal states (Table 2). Models with suffix *visc* have different reference viscosities or viscosity structures to investigate the influence of convection vigor and surface velocities on mantle differentiation. Lastly, with models *03_depltd*, *05_depltd*, and *07_depltd*, the initial amount of HPEs present within the convecting mantle is varied, so that the impact of changing the amount of radiogenic heat input is tested.

3.1.1. Effects of Viscosity

Surface velocities are controlled by the vigor of convection, itself scaled by the viscosity and its structure. Models with higher reference viscosities and a viscous lid (*1_22_visc*, *3_22_visc* and *10_lid_visc*, respectively) have a lower Rayleigh number and tend to retain their heat, as witnessed by the evolution of their average temperature (Figure 1a) and the reduced surface heat flux (Figure 1b). Indeed, models with higher viscosities maintain a positive heat budget (still heating up) for longer because heat is retained and the heat provided by HPEs (particularly ^{40}K) accumulates (Figure 1c). We note that the effect of a viscous lid is of secondary importance in comparison to the effects of the reference viscosity, though significant given the low contrasts investigated (Figure 1). Conversely, with a lower reference viscosity and higher surface velocities, the mantle can get rid of its heat more efficiently: the surface heat flux is higher (Figure 1b) and the heat budget reaches more negative values

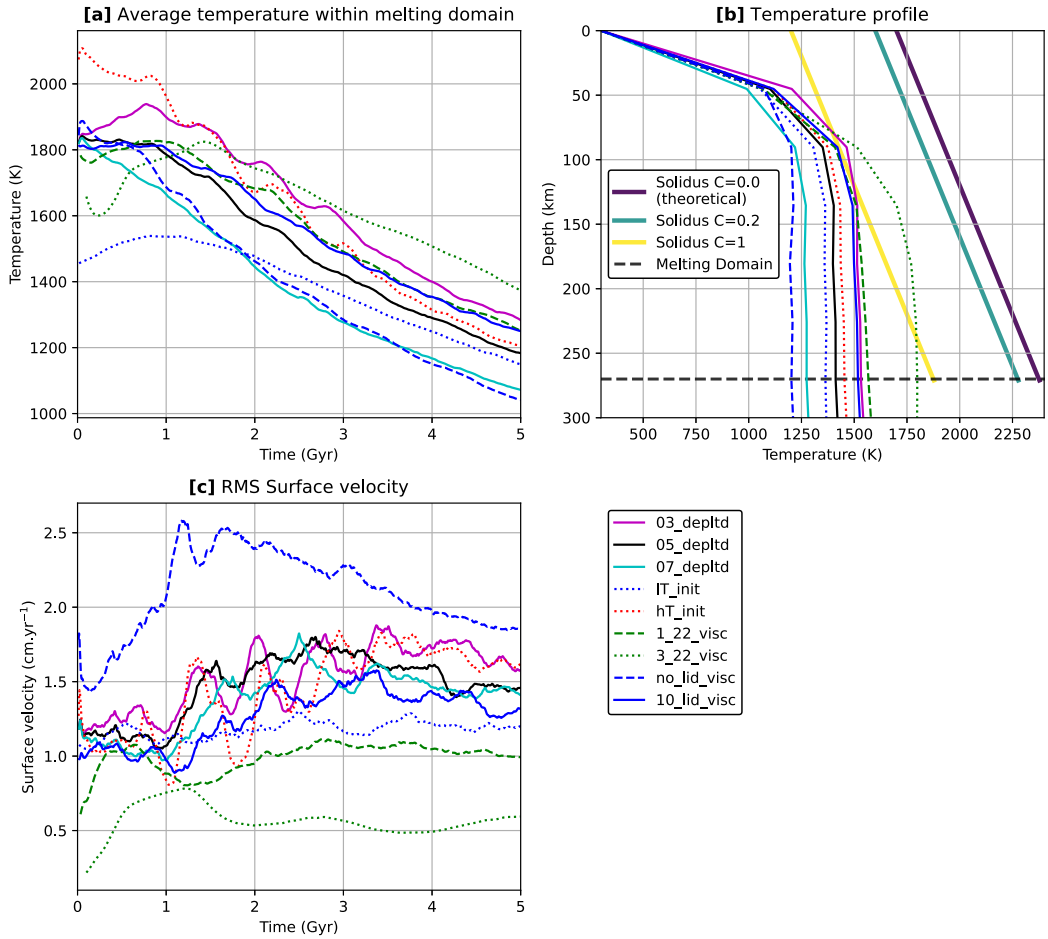

Figure 2. Temperature within the melting domain and surface velocity. (a) Average temperature within the melting domain (volume average) as a function of time. (b) Temperature profiles in the uppermost mantle at 4.5 Gyr and solidii (Yellow for $C = 1$, Blue for $C = 0.2$ and purple for theoretical $C = 0$ solidus). Horizontal black dashed line in (b) shows the base of the imposed melting domain. (c) Root Mean Square surface velocity as a function of time.

earlier in the simulation (Figure 1c). Temperature profiles in Figure 2b show the capability to retain heat as the temperature of the advective zone (i.e., the zone where the advective heat flux is dominant and characterized by a low temperature gradient) increases with reference viscosity and with the viscosity of the lid to a lesser extent.

The evolution of the average temperature within the melting domain (i.e., where the mantle can melt, the uppermost 270 km) (Figure 2a) is similar to that of the global average temperature (Figure 1a) for all models except case *3_22_visc*. This is explained by the significant change in the thermal structure (Figure 2b). Indeed, the thickness of the TBL (i.e., the conductive lid, characterized by a high temperature gradient) increases with the reference viscosity. The average temperature within the melting domain is thus strongly dependent on the thickness of the TBL. It also means that the average advection velocities are reduced when the TBL thickness is increased (Figure 2c), causing greater residence time of material within the melting domain. Comparing case *3_22_visc* to the reference (*05_depltd*), the average temperature of *3_22_visc*, whether it is within the melting domain or of the whole mantle, is higher than reference case (Figures 1a and 2b). However the average temperature within the melting domain is closer to reference than the whole mantle average is, this is due to the thicker TBL of *3_22_visc*. The fact that the melting domain is located in the uppermost mantle has a buffering effect on the average temperature differences between models in the melting domain. This effect is due to the presence of the TBL with the shared surface boundary condition ($T_S = 300\ K$, Table 1).

Variations in the reference viscosity therefore produce distinct thermal evolutions, with strong differences in average mantle temperature (Figures 1a and 2a). However, the surface heat flow values become less distinct

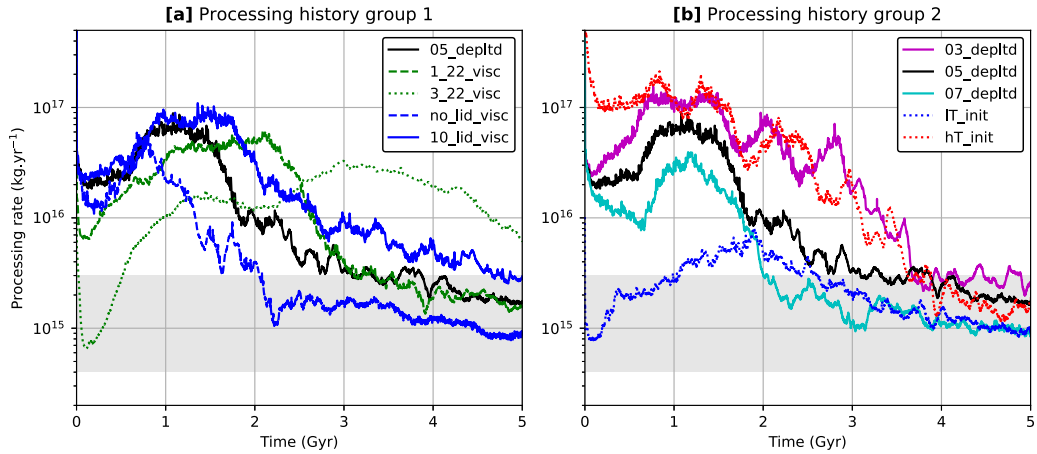

Figure 3. Processing rates as a function of time for presented simulations. (a) Gathers models where reference viscosity and viscosity of the lid are varied. (b) Shows models with different initial thermal states and heat-producing elements concentrations. The shaded area (a, b) represents the range of estimates for the current processing rate of the mantle.

toward the end of the simulation (after 4 Gyr, Figure 1b), and also for the net heat budget (Figure 1c). The previous observations translate into the processing rates (Figure 3a) as follows. Variations in the reference viscosity cause the most distinct evolution of the processing rates, which can be attributed to the thermal evolution. Indeed, the maximum processing rate is significantly delayed when reference viscosity is increased because of the ability of viscous models to maintain higher average mantle temperature (Figures 2a and 3a). When the viscosity is decreased, advection velocities are greater (resulting in lower residence time within the melting domain) and the TBL is thinner, which promotes higher processing rates (Figure 3a). That is why, early in the simulation, when average temperature peaks and the mantle is fertile, the processing rates of cases with low reference viscosity reach high values. However, because these models are also more efficient at releasing their heat, their processing rates decrease faster (Figure 3a). This effect is well illustrated by models testing the viscosity of the lid (*no_lid_visc*, *05_depltd*, and *10_lid_visc*). The presence of a lid causes the surface velocity to drop and the temperature to rise, proportionally to its strength (Figure 2): the processing rates are higher (Figure 3a). Conversely, without a lid (case *no_lid_visc*), the average temperature is lower as surface velocities are not restrained and processing rates decrease (Figure 3a). As the viscosity controls the amount of heat retained and advection velocities, different patterns of processing histories (i.e., temporal evolution of processing rates) can be produced by using different viscosities (e.g., reference viscosity and viscosity of the lid).

3.1.2. Different Thermal Evolution, Same Viscosity

The impact of the initial thermal state, tested with models *05_depltd*, *lT_init* and *hT_init*, shows a great influence on the evolution of average mantle temperature (of the whole mantle and within the melting domain), surface heat flux and heat budget (Figures 1a–1c and 2a, respectively). The higher the initial mantle temperature the more heat is transferred through the surface (Figure 1b). Similarly, the more the mantle is enriched in HPEs, the more radiogenic heat is provided throughout the simulation (the net cooling is delayed or shortened by increasing or decreasing the amount of HPEs, respectively; Figure 1c), and the higher the average temperature and surface heat flow (Figures 1a, 1b, and 2a). The temperature of the advective zone in Figure 2 is proportional to the amount of HPEs and average initial temperature and scales the processing rates (Figure 3b). We note that while the amount of radiogenic heat generally scales with surface velocities, it is not the case for initial thermal states (Figure 2c).

The evolution of average temperature within the melting region is reflected in the processing rates in Figure 3b. The processing rates of cases *lT_init* and *hT_init* (testing the influence of initial temperature) bound cases *03_depltd*, *05_depltd*, and *07_depltd* (testing the influence of HPEs concentration) most of the time. The latter cases show expected offsets due to the relative differences in temperature (due to various amounts of heat provided) but similar trajectories. What we notice about this class of models (group 2, Figure 3b) is that despite their different thermal evolutions, they converge to similar values of processing rate: all reach the Earth's current estimated range at 4 Gyr (Figure 3). As a consequence, the current range of processing rate estimates cannot be

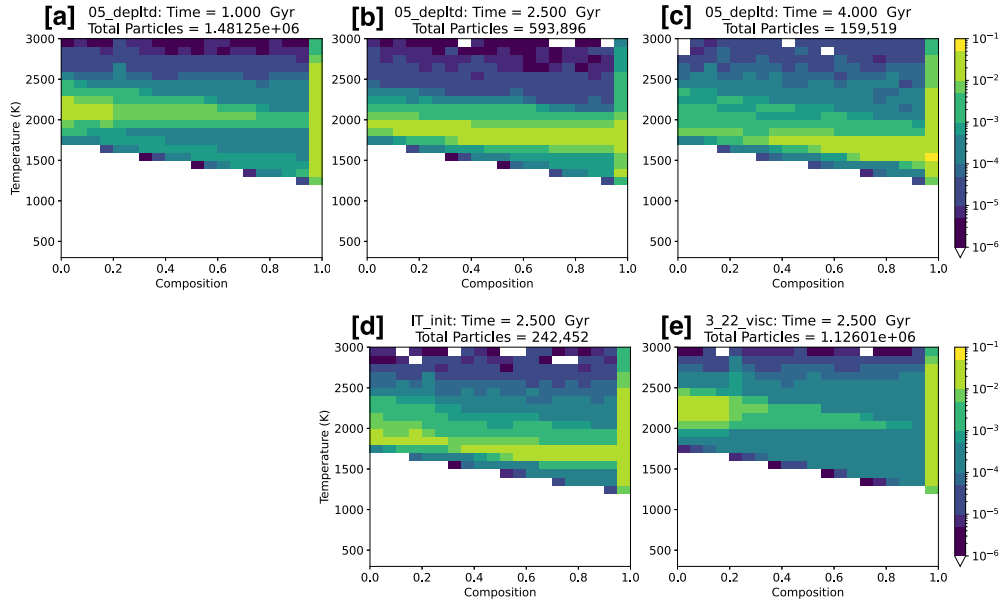

Figure 4. Normalized 2D histograms of the composition and temperature of particles prior to melting for cases *05_depltd* (a–c), *lT_init* (d), and *3_22_visc* (e). Histogram outputs of (a–c) at 1 Gyr, 2.5 Gyr, and 4 Gyr, respectively and (d) and (e) at 2.5 Gyr. Bin count is normalized to the total number of melting particles, displayed below each histogram title. If a particle's temperature exceeds the limit of $3,000\ K$ imposed by the bin range, it is counted in the highest temperature bin. Each panel shows which classes of compositions are sampled by melting (as a function of their C value) and their temperatures. For example, (a) shows that the heterogeneities sampled by melting mostly have high temperature and are largely depleted ($C < 0.2$) or highly enriched ($C > 0.95$).

used to distinguish between models (Figure 3). For models testing the influence of initial temperature, the convergence is also observable in temperatures and surface heat flow (Figures 1a, 1b, and 2a), illustrating the ability of the dynamic system (driven by shared parameters, e.g. viscosity structure) to mask the influence of the initial condition during Earth's lifespan. Therefore we show that the amount of HPEs and the initial thermal state are determining parameters for the processing history of the mantle while they do not induce a lot of variability in the processing rates after 4 Gyr.

3.2. Preferential Sampling Controlled by Mantle Temperature

The role of temperature is critical to the processing rates because it dictates the degree of melting and the types of material that can melt. To visualize what material is sampled in the melting domain, we produce 2D histograms of particles (tracers) that are about to be melted as a function of their bulk composition (C) and temperature (Figure 4). Figure 4 panels a–c show successive time snapshots of these particles prior to melting from reference case (model *05_depltd*). Panels d and e show models *lT_init* and *no_lid_visc* at 2.5 Gyr, respectively. A first observation is that the average temperature of the sampled particles decreases as the simulation advances (Figures 4a–4c), as the mantle is cooling (Figure 2a). This example highlights that the temperature of the mantle controls the range of composition that can be sampled by melting. Indeed, with a composition-dependent solidus, higher temperatures allow less fertile material (with a low C) to be melted, increasing the range of composition that can possibly melt. Additionally, higher temperatures leads to further depletion of more fertile compositions, as the temperature excess between the material's actual temperature and its solidus is greater (Figure 2b). Therefore increasing the temperature results in more material being processed in the melting domain and more depletion, causing the processing rate to increase. Conversely, reducing the temperature of the melting domain restrains the range of compositions that are allowed to melt and depletion is minimized and so processing rates are lower (case *lT_init*, Figure 4d). We note that melting, as it is implemented (van Heck et al., 2016), tends to produce the two end-member compositions extensively and much less of intermediate compositions (Figure S3 in Supporting Information S1). Therefore, there are three dominant compositions: fully depleted ($C = 0$), fully

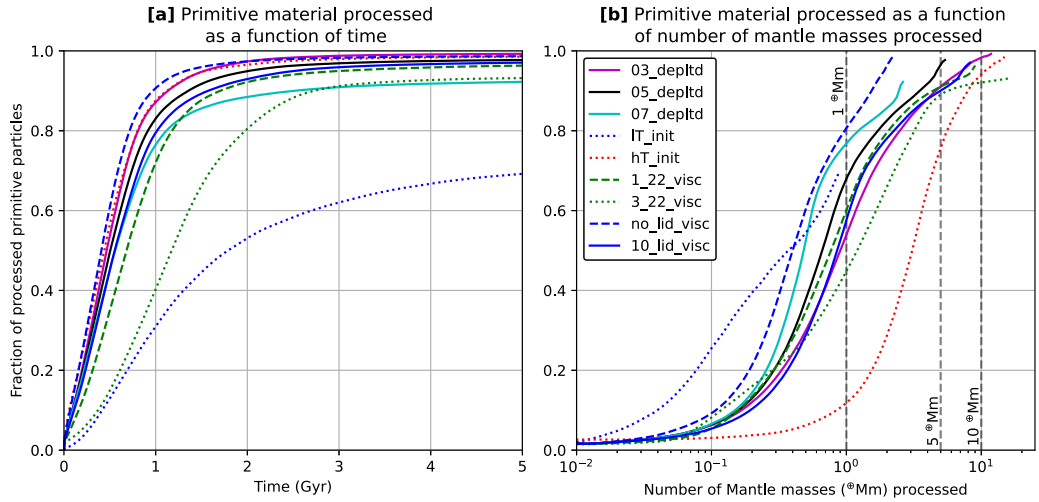

Figure 5. Proportion of primitive particles processed as a function of time (a) and number of equivalent Earth mantle masses processed (b).

enriched ($C = 1$) and initial primitive undegassed material ($C = 0.2$). As fully depleted material cannot produce melt, it cannot appear in the histograms (Figure 4).

Simultaneously, the viscosity structure of the melting domain can change the dynamics radically. The thickness of the TBL and surface velocities both control not just the thermal structure of the shallow mantle but also the type of material that is going to be processed. Two end-member melting regimes arise: The "plume melting regime" (Figures 4a and 4e), characterized by the preferential sampling of both highly enriched and depleted compositions at high temperatures (high difference between the melting particles' temperature and their respective solidus). On the other hand, the "decompression melting regime" (Figures 4c and 4d) is characterized by a more evenly distributed sampling of the whole range of composition at lower temperature (low temperature excess compared to their respective solidus). The former is favored in viscous simulations (e.g., *1_22_visc*, *3_22_visc*, and *10_lid_visc*), where heat is retained in the mantle and the upper TBL is thicker. Such dynamical context favors development of strong plumes that carry high temperature basaltic and harzburgitic material (Supplementary videos SV4, SV5, and SV7, https://doi.org/10.5285/77d69231-7748-4145-a5d6-2b2a59d19cda). The "plume melting regime" is associated with high processing rates (total count of melting particles, Figure 4). The "decompression melting regime" is favored in least viscous simulations (e.g., late *05_depltd*, *no_lid_visc*, and *lT_init*), where material within the melting domain can be renewed frequently and fast enough, and can reach shallow regions so that the least fertile compositions can be processed. Supplementary videos (late SV1, SV6, and SV8, https://doi.org/10.5285/77d69231-7748-4145-a5d6-2b2a59d19cda) show that for this meting regime, plumes are generally weaker, so their signature doesn't overprint the histogram (Figure 4).

3.3. Preservation of the Primitive Undegassed Mantle

Figure 5 displays the proportion of primitive undegassed material that has been processed/melted as a function of time (Figure 5a) and number of mantle masses processed by melting (logarithmic scale, Figure 5b). As shown in Figure 3, the processing history can be more or less intensive. A consequence of this is that the amount of processing (i.e., the integral of the processing rates over the running time, here expressed in mantle masses), is greatly affected by the parameters explored and therefore it is an important consideration for the preservation of primitive undegassed material (i.e., material that has not been processed by melting). Understandably, preserving the primitive mantle is easier when only one mantle mass has been processed compared to 10 or more. That is the reason why model *lT_init* can preserve more than 30% of its primitive material after 5 Gyr; the processing of the mantle, conditioned by its dynamics, favors preservation. We find that, among the models that have the same viscosity setting (i.e., *lT_init*, *hT_init*, *03_depltd*, *05_depltd*, and *07_depltd*), the models that have undergone the least processing over their history perform best at preserving the primitive mantle (Figures 3 and 5a).

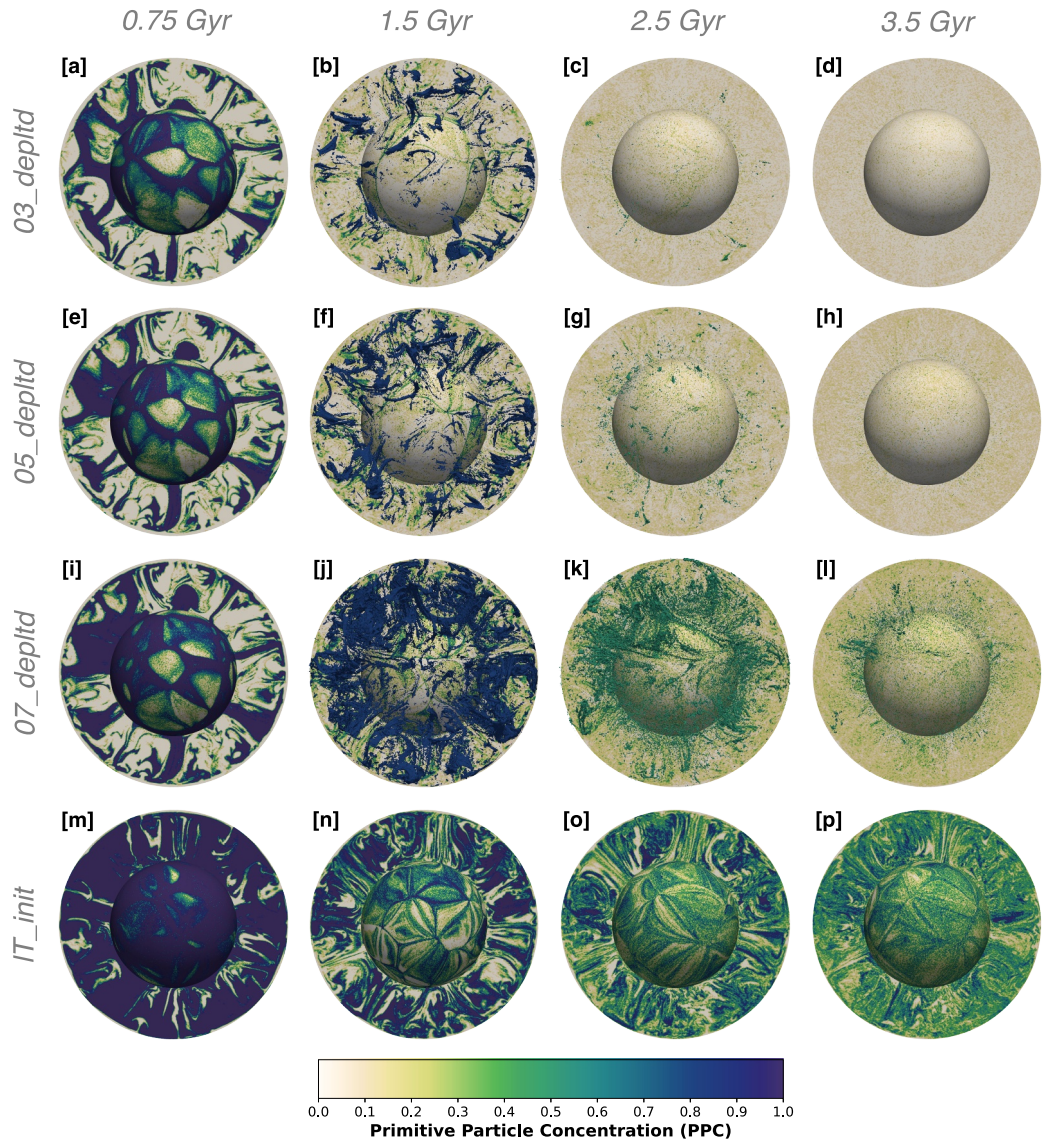

Figure 6. Visualizations showing the primitive particle concentration (PPC, i.e. the fraction of primitive undegassed particles to the total number of particles owned by each grid node) for models testing radiogenic heat input: *03_depltd* (a–d), *05_depltd* (e–h), *07_depltd* (i–l) and low initial temperature model *lT_init* (m–p) at different times: (a, e, i, m) 0.75 Gyr, (b, f, j, n) 1.5 Gyr, (c, g, k, o) 2.5 Gyr and (d, h, l, p) 3.5 Gyr. Isocontours on panels (b, f, j) show PPC of 0.8 and isocontours of panels (c, d, g, h, k, l) PPC of 0.5.

However, the preservation of the primitive undegassed mantle depends upon more than the integrated amount of processing, as shown by the pairs of models *07_depltd* with *no_lid_visc* and *hT_init* with *3_22_visc*. Each pair reaches similar numbers of mantle masses processed at the end of the simulation (about 3 and 13 mantle masses, respectively; Figure 5b) but displays different degrees of preservation of primitive material (Figure 5a). Again, we find that the processing history is the dominant determining factor. Different patterns of processing history show variations in the way primitive material is sampled (resulting in different slopes in Figure 5a). Specifically, lower processing rates early in the simulation favors preservation of the primitive material (case *lT_init*, *3_22_visc*, and *07_depltd* Figures 3 and 5a). As the primitive material is heated by the HPEs it holds and receives heat from the Core-Mantle Boundary (CMB), the primitive material of the lower mantle is likely to become strongly buoyant early in the simulation. As the primitive material collects in upwellings (Figure 6 and Figure S4 in Supporting Information S1, supplementary SV1-9, https://doi.org/10.5285/77d69231-7748-4145-a5d6-2b2a59d19cda), it will reach the melting domain with a high temperature and therefore melt (supplementary SV1-9, https://doi.org/

10.5285/77d69231-7748-4145-a5d6-2b2a59d19cda). For that reason, the first 1.5 Gyr are critical for the preservation of primitive material. That is one of the reasons why model *07_depltd*, with less HPEs, better preserves primitive material than *03_depltd* and *05_depltd*. Additionally, the presence of a viscous lid and its strength cause significant differences in the total amount of processing, but there is little difference in the amount of primitive material preserved at the end of the simulation (Figure 5b). The presence of a strong lid (model *10_lid_visc*) induces slightly better preservation of primitive material but a higher amount of processing (about 8 mantle masses, Figures 3a and 5).

The asymptotic character of the curves of Figure 5a shows that primitive material is not as efficiently sampled past 1.5 Gyr for most cases. It is attributed first to the availability of primitive material. As the primitive material is processed, it becomes less abundant and less likely to be sampled by melting. Therefore, the proportion of processed primitive material never truly reaches 1, even when the processing is very intensive, for example case *hT_init* where more than 10 mantle masses have been processed by 5 Gyr (Figure 5a). Yet model *lT_init* illustrates another operating mechanism. As primitive material remains abundant throughout the simulation in this case, the decrease in the slope of the fraction of processed primitive material (Figure 5a) is due to the thermal evolution. Indeed, as the average mantle temperature decreases, exceeding the solidus for the primitive material ($C = 0.2$) is less likely, so less primitive material is sampled (Figure 4). Visualizations in Figure 6 show the Primitive Particle Concentration (PPC), that is the ratio of the number of primitive undegassed particles owned by a node (grid point) to the total number of particles owned by the same node. The PPC allows us to observe the competition between the mixing (and stirring) and the sampling of primitive material in the melting domain. For the presented models in Figure 6, the processing rates peak within the first 1.5 Gyr, before they decrease for the rest of the simulation (Figure 3b). The first snapshots at 0.75 Gyr (first column Figure 6), show distinct regions where primitive material is concentrated (PPC $\simeq$ 1) and others where it is totally absent (PPC $\simeq$ 0). As the simulation advances, we observe the model transitioning from that contrasted state to a more mixed state (re-homogenization of bulk composition Figure S5 in Supporting Information S1), where primitive material is better distributed across the volume of the mantle. The PPC value globally decreases of course, because the primitive material is processed but also because mechanical stirring and mixing homogenizes the PPC (Figure 6). We note that the plumes of the presented models are quite stable throughout the simulation (limited lateral wandering, supplementary videos SV1-9, https://doi.org/10.5285/77d69231-7748-4145-a5d6-2b2a59d19cda), which leads to regional differences in PPC (e.g., Figures 6g, 6k, and 6l). This dynamical behavior might favor preservation of geochemical heterogeneities.

The primitive undifferentiated undegassed mantle, enriched in HPEs, is initially hotter than the early generated compositional heterogeneities mainly located in the upper mantle. As the simulation advances, the primitive undegassed material of the lower mantle is collected in upwellings (Figure 6 and Figure S4 in Supporting Information S1, supplementary SV1-9, https://doi.org/10.5285/77d69231-7748-4145-a5d6-2b2a59d19cda), which will ultimately lead to its sampling once plumes reach the melting domain. The surviving primitive undegassed material is scattered across the mantle volume by convective mixing, which forces its temperature to converge to the average mantle temperature. Both sampling hot primitive undegassed material and mixing the remaining undegassed material contribute to faster cooling of this heterogeneity. Therefore, the thermal evolution (temporal variation of the average mantle temperature) is crucial to the survival of the primitive undegassed material. Equally, so is the efficiency of convective mixing.

4. Discussion

The results show that processing rates are influenced by the temperature of the mantle. Most importantly, the ability of the mantle to evacuate heat is key in determining the processing rate and its evolution. Therefore, mantle dynamics, by dictating the thermal evolution, controls mantle differentiation. That means that the vigor of convection, here mainly controlled by the viscosity, is determinant. If the mantle is convecting fast (high surface velocities) and the TBL is thin, the processing rates will start high as the material within the melting domain is renewed quickly. However, this geodynamical context also promotes an efficient cooling of the mantle, leading to reduced processing rates as they follow the average temperature evolution (Coltice et al., 2009). Conversely, with more sluggish convection (slower surface velocities and thicker TBL), the processing rates are not as high initially but maintain themselves as heat is retained in the mantle (Figure 3). Also, the type of material that is sampled by melting is controlled by mantle dynamics (i.e., sub-ridge and plume dynamics, Figure 4). We therefore suggest that the convective regime has great influence on the processing history and preservation of heterogeneities

(Coltice et al., 2009; Lourenço et al., 2020; Stevenson, 2003). Based on the trends highlighted by our results, we speculate that in the case Venus was a stagnant-lid planet, it would have a processing history (Figure 3a) and a melting regime (plume melting regime, Figure 4) that would favor preservation of long-term heterogeneities. Equally, planet size would be a major control (Stevenson, 2003). Smaller planets (e.g., Mars), with a radius half that of the Earth, would have a stagnant lid, much less vigorous convection and would have received much less heat during its formation, all factors promoting preservation of ancient heterogeneity.

Additionally, the actual processing history of the Earth's mantle could be more complex than in the presented generic models, as the onset of plate tectonics (Cawood et al., 2018; Palin et al., 2020) and the associated change of convective regime (Cawood et al., 2022; Lenardic, 2018) are still debated. We suggest that processing rates are unlikely to have been constant through Earth history. Nonetheless, the amount of ^{40}Ar (daughter of ^{40}K, one of the main HPEs with a half-life of 1.25 Gyr) degassed into the atmosphere should agree with the processing history (Zhang et al., 2023). Modeling the outgassing of ^{40}Ar requires further considerations, for example the buoyancy of recycled oceanic crust and the extraction and recycling of the continental crust (Bender et al., 2008; Guo & Korenaga, 2020; J. Huang & Davies, 2007a, 2007b, Tucker et al., 2022), which can be investigated in further studies. Part of the limitations of the presented models reside in the fact that they are run for 5 Gyr and that the effects of temperature dependent viscosity are not taken into account. Potential effects could result in more efficient cooling and mixing early in the simulation but less efficient later on, which could lead to a favorable processing history. Another consequence is that the impact of the initial thermal state is only partially evaluated with models *lT_init* and *hT_init*. Furthermore, the presented models probably do not capture the most realistic dynamics, especially in the earliest stages of the simulation. We have shown that the conditions of this stage have a strong effect on the subsequent fate of primitive undegassed material and long-term heterogeneities (Figure 5; J. Huang & Davies, 2007b) but it is also poorly constrained (little geological evidence). However, not considering temperature dependent viscosity allows the analysis of the separate influence of temperature and viscosity on processing rates (Figures 2 and 3).

Another limitation is that models lack plate-like behavior (yield stress rheology not included, van Heck and Tackley (2008)) and surface velocities are not quite Earth-like. This is important to mention as the results show significant sensitivity to surface velocity and viscosity (cases *no_lid_visc*, *05_depltd*,and *10_lid_visc*). The presented models have weak lithospheres, which allows us to investigate a range of surface velocities but these models display diffuse surface deformations as opposed to the narrow localized deformation of the plate-like mobile lid regime. It is clear that a more Earth-like surface rheology with stronger lithosphere could have significant influence on thermal evolution and sublithospheric mantle flow (Foley & Becker, 2009; J. Huang et al., 2003; Xiang et al., 2025). We suspect that plate-like behavior would further favor mixing efficiency in the asthenospheric mantle leading to higher processing rates (at least initially) and more decompression melting. Future studies could investigate the influence of surface rheology on the type of heterogeneities processed by melting and mantle differentiation. Nonetheless, we take satisfaction in the fact that models with the same viscosity structure (*05_depltd*, *03_depltd*, *07_depltd*, *lT_init* and *hT_init*, $\eta_{ref} = 5.10^{21}$ Pa.s) share similar surface velocities (1.5 ± 0.2 cm.yr^{-1} Figure 2c, bounded by viscosity induced variations; Rayleigh number of $\simeq 10^8$). Moreover, this group of simulations also succeeds in converging within the range of Earth's current processing rate estimates after 4 Gyr of simulation (Figure 3b). The weak sensitivity of late processing rates to the initial temperature and initial HPEs concentration is surprising given the large variations imposed by the parameter space (Table 2), yet it suggests that we, as geodynamicists, must be careful of the processing history (the amount of processing) we impose on our models when investigating the survival of long-term heterogeneities, as we might impose dynamics that either favors preservation of material or its sampling. Jones et al. (2021) also observed the influence of the amount of processing on survival of ancient heterogeneity. Accordingly, we suggest that realistic radiogenic heating (non constant and if possible spatially heterogeneous) is crucial to improve model accuracy and resulting interpretation of the preservation of long-lived heterogeneities (in agreement with Panton et al. (2023)).

The parametrization of the solidus is highly simplified in the presented models and differs from previous experimental estimations and parametrizations (e.g., Katz et al., 2003; Yasuda et al., 1994). The choice of parametrization affects both global processing rates and processing of specific heterogeneities (e.g., primitive undegassed material, basaltic material) via the amount of depletion and the range of composition that can melt. However the results analysis is mainly comparative, and because all models share the same solidus

parametrization, it is expected that the observed trends and conclusions should remain valid. Previous mentioned limitations can cause the model to be potentially conservative in terms of processing (e.g., low average temperatures, solidus parametrization, lack of temperature dependent viscosity and plate-like rheology). However, the amount of processing of the majority of the models is higher compared to other studies (e.g., Jones et al., 2021; Tucker et al., 2022). On the other hand, models do not consider heat transfer associated with melting events, which could have a significant impact on mantle cooling, especially during the first 2 Gyr (Xie & Tackley, 2004), potentially favoring preservation. Despite limitations, presented models suggest that mantle mixing is highly efficient, as previously noted by Coltice (2005) and Ferrachat and Ricard (1998), preservation of primitive undegassed material is thus challenging in most cases. This could be indicative that additional physical mechanisms need to be invoked (e.g., density and/or viscosity contrast) in order to explain primitive signatures and counter the effects of mixing (for example, Ballmer et al., 2017; Gülcher et al., 2020, 2021; Jones et al., 2021). Nonetheless, results suggest that mixing can act simultaneously against and in favor of preservation of primitive undegassed material, as it efficiently scatters heterogeneities across the mantle and promotes cooling, respectively.

In agreement with previous studies (J. Huang & Davies, 2007a, 2007b), we find that the "processing time" (i.e., the time needed to process the equivalent of one mantle mass) is key for primitive material survival. The temperature and buoyancy of primitive material reach their maximum in the first 1.5 Gyr of the simulation. As the mantle cools and the remaining primitive material is scattered across the mantle volume, the primitive undegassed material temperature tends toward that of the average mantle; it becomes less likely to be processed. If the thermal evolution allows it, for example case *07_depltd*, *lT_init*, the cooling is such that the sampling of the primitive undegassed material becomes difficult (because the solidus $C = 0.2$ is fixed Figure 2b). In those cases, primitive material could only be processed in rare occurrences when the material's temperature is significantly higher than the average mantle (typically plumes). Consequently, more undegassed signatures would appear in magmatism that is associated with upwellings. Whether this mechanism is operating in the Earth and partly responsible for the dichotomy between MORBs and OIBs is unclear, because of model assumptions (simplified solidus, lack of both plate-like behavior and decompression melting). More constraints on thermal evolution appear crucial to better understand the fate of the primitive undegassed mantle (G. F. Davies, 2009; Herzberg et al., 2010; Korenaga, 2018). We remind the reader that primitive material neither had any excess density nor any excess viscosity in the presented simulations. While the effects of density and viscosity can keep the material out of the melting domain forming structures in the lower mantle (e.g., termo-chemical piles, BEAMS), they would also maintain a positive thermal anomaly of the primitive material as well as resistance against dispersing across the mantle (Gülcher et al., 2021).

Variability exists on the value of the estimated ratios of HPEs of the BSE (e.g., the value of the K/U ratio, Arevalo et al., 2009; McDonough & Sun, 1995; Palme & O'Neill, 2014), as the extent of depletion on Earth of the moderately volatile element K is not tightly constrained. A lower K budget would reduce the amount of radiogenic heat provided to the mantle (especially in the first couple Gyr of Earth history), favoring better preservation of long-term heterogeneities according to our results. It would also help reduce the amount of "missing ^{40}Ar" (Tucker et al., 2022). Accordingly, previous BSE elemental budget reconstructions advocated for significant lower K content (Jackson & Jellinek, 2013; Lyubetskaya & Korenaga, 2007a, 2007b). Nevertheless, we suggest that the extraction of the continental crust could be a more significative process to remove HPEs from the convecting mantle. Due to overall incompatible behavior of HPEs, they concentrate in the continental crust (Cawood et al., 2022; Y. Huang et al., 2013; Rudnick & Gao, 2003) so that c.a. half of the K budget is in the continental crust. While the timing of the extraction of the continental crust is still debated (Hawkesworth et al., 2019), more recent works by Guo and Korenaga (2023), Guo and Korenaga (2020) favor the early extraction scenario, previously supported by Armstrong (1991). Despite uncertainties also persisting on the continental crust's recycling and generation rates over time (Cawood et al., 2022), an early extraction coincides with significant removal of HPEs (at a decisive time for the primitive undegassed material) that would promote a more favorable processing history for better preservation of long-term geochemical heterogeneities.

5. Conclusion

In this work, we investigated the role of mantle dynamics in controlling the processing rate of the mantle and the implications for the preservation of the primitive undegassed mantle using 3D convection models. In agreement with previous studies, we find that the amount of processing, although poorly constrained, is crucial for the

survival of long-term geochemical heterogeneities. Results show that thermal evolution, controlled by the ability of the mantle to evacuate its heat, dictates the processing history of the mantle. The type of material that is processed in the melting the melting domain is controlled by temperature and surface dynamics, suggesting strong control of the convective regime. The current heat flow and processing rate estimates cannot be used to distinguish between different processing histories. However, the survival of primitive undegassed mantle is strongly dependent on the processing history, as simulations present between $\leq$1% and 30% of preserved primitive material. Its preservation is favored by reducing the total amount of processing, particularly in the first half of Earth history. Such a situation is achieved with reduced mantle HPEs concentration, lower initial thermal state and a more viscous lid. The surviving primitive undegassed mantle is dispersed by efficient mixing and stirring so its temperature ultimately converges toward that of the average mantle. Therefore, the thermal evolution is key to the survival of the primitive undegassed mantle.

Conflict of Interest

The authors declare no conflicts of interest relevant to this study.

Availability Statement

Open research results generated for this study are available at: https://doi.org/10.5285/9bcf2d04-3f29-4ff1-9089-06cb99da7316 (Récalde et al., 2025a). These files contain Paraview visualization files at 50 Myr intervals for each model and complementary files used to produce the manuscript figures (see README.md for details). The TERRA code used in this study predates open-source licensing. Therefore, we do not have the rights to release all parts of the code, yet segments which have been implemented for this study are available upon request. Instead, we provide the parameter file, the compiled executable, restart files and instructions to reproduce each simulation of this study in the data set. Supplementary videos (SV1: *05_depltd*, SV2: *03_depltd*, SV3: *07_depltd*, SV4: *1_22_visc*, SV5: *3_22_visc*, SV6: *no_lid_visc*, SV7: *10_lid_visc*, SV8: *lT_init*, and SV9: *hT_init*) are available at https://doi.org/10.5285/77d69231-7748-4145-a5d6-2b2a59d19cda (Récalde et al., 2025b). Left panel shows temperature anomalies (compared to layer average) and right panel the Primitive Particle Concentration (PPC, i.e. the fraction of primitive undegassed particles to the total number of particles owned by each grid node) through simulation time (50 Myr intervals from 0.05 to 5 Gyr).

Acknowledgments
This research was funded by the NERC large grant "Mantle Circulation Constrained (MC2): A multidisciplinary 4D Earth framework for understanding mantle upwellings" (Grant NE/T012633/1), the grant "Feedbacks between mineral reactions and mantle convection" (Grant NE/V018221/1) and by the School of Earth and Environmental Sciences, Cardiff University. This work used the ARCHER2 UK National Supercomputing Service (Beckett et al., 2024; https://www.archer2.ac.uk). Graphs were produced using the Matplotlib package (Hunter, 2007) and visualizations were produced using the ParaView software (Ayachit, 2015). The authors thank the two anonymous reviewers for providing insightful comments that improved the manuscript. This is Cardiff EARTH CRediT Contribution 48.

References

Albarède, F., & van der Hilst, R. D. (2002). Zoned mantle convection. *Philosophical Transactions of the Royal Society of London, Series A*, *360*(1800), 2569–2592. https://doi.org/10.1098/rsta.2002.1081

Allègre, C. J., & Turcotte, D. L. (1986). Implications of a two-component marble-cake mantle. *Nature*, *323*(6084), 123–127. https://doi.org/10.1038/323123a0

Arevalo, R., McDonough, W. F., & Luong, M. (2009). The K/U ratio of the silicate Earth: Insights into mantle composition, structure and thermal evolution. *Earth and Planetary Science Letters*, *278*(3), 361–369. https://doi.org/10.1016/j.epsl.2008.12.023

Armstrong, R. L. (1991). The persistent myth of crustal growth. *Australian Journal of Earth Sciences*, *38*(5), 613–630. https://doi.org/10.1080/08120099108727995

Ayachit, U. (2015). *The ParaView guide: A parallel visualization application*. Kitware, Inc.

Ballmer, M. D., Houser, C., Hernlund, J. W., Wentzcovitch, R. M., & Hirose, K. (2017). Persistence of strong silica-enriched domains in the Earth's lower mantle. *Nature Geoscience*, *10*(3), 236–240. https://doi.org/10.1038/ngeo2898

Baumgardner, J. R. (1985). Three-dimensional treatment of convective flow in the earth's mantle. *Journal of Statistical Physics*, *39*(5), 501–511. https://doi.org/10.1007/BF01008348

Baumgardner, J. R., & Frederickson, P. O. (1985). Icosahedral discretization of the two-sphere. *SIAM Journal on Numerical Analysis*, *22*(6), 1107–1115. https://doi.org/10.1137/0722066

Becker, T. W., Kellogg, J. B., & O'Connell, R. J. (1999). Thermal constraints on the survival of primitive blobs in the lower mantle. *Earth and Planetary Science Letters*, *171*(3), 351–365. https://doi.org/10.1016/S0012-821X(99)00160-0

Beckett, G., Beech-Brandt, J., Leach, K., Payne, Z., Simpson, A., Smith, L., et al. (2024). ARCHER2 service description (Technical Report). *Zenodo*. https://doi.org/10.5281/zenodo.14507040

Bender, M. L., Barnett, B., Dreyfus, G., Jouzel, J., & Porcelli, D. (2008). The contemporary degassing rate of ^{40}Ar from the solid Earth. *Proceedings of the National Academy of Sciences*, *105*(24), 8232–8237. https://doi.org/10.1073/pnas.0711679105

Bennett, V. C., Brandon, A. D., & Nutman, A. P. (2007). Coupled 142Nd-143Nd isotopic evidence for Hadean mantle dynamics. *Science*, *318*(5858), 1907–1910. https://doi.org/10.1126/science.1145928

Bercovici, D., Schubert, G., & Glatzmaier, G. A. (1989). Influence of heating mode on three-dimensional mantle convection. *Geophysical Research Letters*, *16*(7), 617–620. https://doi.org/10.1029/GL016i007p00617

Bunge, H.-P., Richards, M. A., & Baumgardner, J. R. (1997). A sensitivity study of three-dimensional spherical mantle convection at 10^8 Rayleigh number: Effects of depth-dependent viscosity, heating mode, and an endothermic phase change. *Journal of Geophysical Research*, *102*(B6), 11991–12007. https://doi.org/10.1029/96JB03806

Cawood, P. A., Chowdhury, P., Mulder, J. A., Hawkesworth, C. J., Capitanio, F. A., Gunawardana, P. M., & Nebel, O. (2022). Secular evolution of continents and the Earth System. *Reviews of Geophysics*, *60*(4), e2022RG000789. https://doi.org/10.1029/2022RG000789

Cawood, P. A., Hawkesworth, C. J., Pisarevsky, S. A., Dhuime, B., Capitanio, F. A., & Nebel, O. (2018). Geological archive of the onset of plate tectonics. *Philosophical Transactions of the Royal Society A: Mathematical, Physical and Engineering Sciences*, *376*(2132), 20170405. https://doi.org/10.1098/rsta.2017.0405

Christensen, U. R., & Hofmann, A. W. (1994). Segregation of subducted oceanic crust in the convecting mantle. *Journal of Geophysical Research*, *99*(B10), 19867–19884. https://doi.org/10.1029/93JB03403

Coltice, N. (2005). The role of convective mixing in degassing the Earth's mantle. *Earth and Planetary Science Letters*, *234*(1), 15–25. https://doi.org/10.1016/j.epsl.2005.02.041

Coltice, N., Marty, B., & Yokochi, R. (2009). Xenon isotope constraints on the thermal evolution of the early Earth. *Chemical Geology*, *266*(1), 4–9. https://doi.org/10.1016/j.chemgeo.2009.04.017

Davies, D. R., Davies, J. H., Bollada, P. C., Hassan, O., Morgan, K., & Nithiarasu, P. (2013). A hierarchical mesh refinement technique for global 3-D spherical mantle convection modelling. *Geoscientific Model Development*, *6*(4), 1095–1107. https://doi.org/10.5194/gmd-6-1095-2013

Davies, G. F. (2008). Episodic layering of the early mantle by the 'basalt barrier' mechanism. *Earth and Planetary Science Letters*, *275*(3), 382–392. https://doi.org/10.1016/j.epsl.2008.08.036

Davies, G. F. (2009). Effect of plate bending on the Urey ratio and the thermal evolution of the mantle. *Earth and Planetary Science Letters*, *287*(3), 513–518. https://doi.org/10.1016/j.epsl.2009.08.038

Davies, J. H., & Davies, D. R. (2010). Earth's surface heat flux. *Solid Earth*, *1*(1), 5–24. https://doi.org/10.5194/se-1-5-2010

Farley, K. A., Natland, J. H., & Craig, H. (1992). Binary mixing of enriched and undegassed (primitive?) mantle components (He, Sr, Nd, Pb) in Samoan lavas. *Earth and Planetary Science Letters*, *111*(1), 183–199. https://doi.org/10.1016/0012-821X(92)90178-X

Ferrachat, S., & Ricard, Y. (1998). Regular vs. chaotic mantle mixing. *Earth and Planetary Science Letters*, *155*(1), 75–86. https://doi.org/10.1016/S0012-821X(97)00200-8

Ferrachat, S., & Ricard, Y. (2001). Mixing properties in the Earth's mantle: Effects of the viscosity stratification and of oceanic crust segregation. *Geochemistry, Geophysics, Geosystems*, *2*(4). https://doi.org/10.1029/2000GC000092

Foley, B. J., & Becker, T. W. (2009). Generation of plate-like behavior and mantle heterogeneity from a spherical, viscoplastic convection model. *Geochemistry, Geophysics, Geosystems*, *10*(8). https://doi.org/10.1029/2009GC002378

French, S. W., & Romanowicz, B. (2015). Broad plumes rooted at the base of the Earth's mantle beneath major hotspots. *Nature*, *525*(7567), 95–99. https://doi.org/10.1038/nature14876

French, S. W., & Romanowicz, B. A. (2014). Whole-mantle radially anisotropic shear velocity structure from spectral-element waveform tomography. *Geophysical Journal International*, *199*(3), 1303–1327. https://doi.org/10.1093/gji/ggu334

Fukao, Y., & Obayashi, M. (2013). Subducted slabs stagnant above, penetrating through, and trapped below the 660 km discontinuity. *Journal of Geophysical Research: Solid Earth*, *118*(11), 5920–5938. https://doi.org/10.1002/2013JB010466

Guerrero, J. M., Deschamps, F., Li, Y., Hsieh, W.-P., & Tackley, P. J. (2023). Influence of heterogeneous thermal conductivity on the long-term evolution of the lower-mantle thermochemical structure: Implications for primordial reservoirs. *Solid Earth*, *14*(2), 119–135. https://doi.org/10.5194/se-14-119-2023

Gülcher, A. J. P., Ballmer, M. D., & Tackley, P. J. (2021). Coupled dynamics and evolution of primordial and recycled heterogeneity in Earth's lower mantle. *Solid Earth*, *12*(9), 2087–2107. https://doi.org/10.5194/se-12-2087-2021

Gülcher, A. J. P., Gebhardt, D. J., Ballmer, M. D., & Tackley, P. J. (2020). Variable dynamic styles of primordial heterogeneity preservation in the Earth's lower mantle. *Earth and Planetary Science Letters*, *536*, 116160. https://doi.org/10.1016/j.epsl.2020.116160

Guo, M., & Korenaga, J. (2020). Argon constraints on the early growth of felsic continental crust. *Science Advances*, *6*(21), eaaz6234. https://doi.org/10.1126/sciadv.aaz6234

Guo, M., & Korenaga, J. (2023). The combined Hf and Nd isotope evolution of the depleted mantle requires Hadean continental formation. *Science Advances*, *9*(12), eade2711. https://doi.org/10.1126/sciadv.ade2711

Hawkesworth, C., Cawood, P. A., & Dhuime, B. (2019). Rates of generation and growth of the continental crust. *Geoscience Frontiers*, *10*(1), 165–173. https://doi.org/10.1016/j.gsf.2018.02.004

Herzberg, C., Condie, K., & Korenaga, J. (2010). Thermal history of the Earth and its petrological expression. *Earth and Planetary Science Letters*, *292*(1), 79–88. https://doi.org/10.1016/j.epsl.2010.01.022

Heyn, B. H., Conrad, C. P., & Trønnes, R. G. (2018). Stabilizing effect of compositional viscosity contrasts on thermochemical piles. *Geophysical Research Letters*, *45*(15), 7523–7532. https://doi.org/10.1029/2018GL078799

Hilton, D. R., & Porcelli, D. (2003). 2.06—Noble gases as mantle tracers. In H. D. Holland & K. K. Turekian (Eds.), *Treatise on geochemistry* (pp. 277–318). Pergamon. https://doi.org/10.1016/B0-08-043751-6/02007-7

Hoffman, N. R. A., & McKenzie, D. P. (1985). The destruction of geochemical heterogeneities by differential fluid motions during mantle convection. *Geophysical Journal International*, *82*(2), 163–206. https://doi.org/10.1111/j.1365-246X.1985.tb05134.x

Hofmann, A. W. (1997). Mantle geochemistry: The message from oceanic volcanism. *Nature*, *385*(6613), 219–229. https://doi.org/10.1038/385219a0

Hofmann, A. W. (2007). 2.03 - Sampling mantle heterogeneity through Oceanic basalts: Isotopes and trace elements. In H. D. Holland & K. K. Turekian (Eds.), *Treatise on geochemistry* (pp. 1–44). Pergamon. https://doi.org/10.1016/B0-08-043751-6/02123-X

Huang, J., & Davies, G. F. (2007a). Geochemical processing in a three-dimensional regional spherical shell model of mantle convection. *Geochemistry, Geophysics, Geosystems*, *8*(11), Q11006. https://doi.org/10.1029/2007GC001625

Huang, J., & Davies, G. F. (2007b). Stirring in three-dimensional mantle convection models and implications for geochemistry: Passive tracers. *Geochemistry, Geophysics, Geosystems*, *8*(3), Q03017. https://doi.org/10.1029/2006GC001312

Huang, J., Zhong, S., & van Hunen, J. (2003). Controls on sublithospheric small-scale convection. *Journal of Geophysical Research*, *108*(B8), e2025GC012289. https://doi.org/10.1029/2003JB002456

Huang, M., Li, Y., & Zhao, L. (2022). Effects of thermal, compositional and rheological properties on the long-term evolution of large thermochemical piles of primordial material in the deep mantle. *Science China Earth Sciences*, *65*(12), 2405–2416. https://doi.org/10.1007/s11430-021-9950-7

Huang, Y., Chubakov, V., Mantovani, F., Rudnick, R. L., & McDonough, W. F. (2013). A reference Earth model for the heat-producing elements and associated geoneutrino flux. *Geochemistry, Geophysics, Geosystems*, *14*(6), 2003–2029. https://doi.org/10.1002/ggge.20129

Hunter, J. D. (2007). Matplotlib: A 2D graphics environment. *Computing in Science & Engineering*, *9*(3), 90–95. https://doi.org/10.1109/MCSE.2007.55

Irifune, T., & Ringwood, A. E. (1993). Phase transformations in subducted oceanic crust and buoyancy relationships at depths of 600–800 km in the mantle. *Earth and Planetary Science Letters*, *117*(1), 101–110. https://doi.org/10.1016/0012-821X(93)90120-X

Jackson, M. G., Carlson, R. W., Kurz, M. D., Kempton, P. D., Francis, D., & Blusztajn, J. (2010). Evidence for the survival of the oldest terrestrial mantle reservoir. *Nature*, *466*(7308), 853–856. https://doi.org/10.1038/nature09287

Jackson, M. G., & Jellinek, A. M. (2013). Major and trace element composition of the high $^{3}He/^{4}He$ mantle: Implications for the composition of a nonchonditic Earth. *Geochemistry, Geophysics, Geosystems*, *14*(8), 2954–2976. https://doi.org/10.1002/ggge.20188

Jaupart, C., Labrosse, S., Lucazeau, F., & Mareschal, J. C. (2015). 7.06—Temperatures, heat, and energy in the mantle of the Earth. In G. Schubert (Ed.), *Treatise on geophysics* (2nd ed., pp. 223–270). Elsevier. https://doi.org/10.1016/B978-0-444-53802-4.00126-3

Jones, T. D., Sime, N., & van Keken, P. E. (2021). Burying Earth's primitive mantle in the Slab graveyard. *Geochemistry, Geophysics, Geosystems*, *22*(3), e2020GC009396. https://doi.org/10.1029/2020GC009396

Kárason, H., & Van Der Hilst, R. D. (2000). Constraints on mantle convection from seismic tomography. In *The history and dynamics of global plate motions* (pp. 277–288). American Geophysical Union (AGU). https://doi.org/10.1029/GM121p0277

Katz, R. F., Spiegelman, M., & Langmuir, C. H. (2003). A new parameterization of hydrous mantle melting. *Geochemistry, Geophysics, Geosystems*, *4*(9), 1073. https://doi.org/10.1029/2002GC000433

Kellogg, L. H., & Turcotte, D. L. (1987). Homogenization of the mantle by convective mixing and diffusion. *Earth and Planetary Science Letters*, *81*(4), 371–378. https://doi.org/10.1016/0012-821X(87)90124-5

Kellogg, L. H., & Wasserburg, G. J. (1990). The role of plumes in mantle helium fluxes. *Earth and Planetary Science Letters*, *99*(3), 276–289. https://doi.org/10.1016/0012-821X(90)90116-F

Koelemeijer, P., Ritsema, J., Deuss, A., & van Heijst, H.-J. (2016). SP12RTS: A degree-12 model of shear- and compressional-wave velocity for Earth's mantle. *Geophysical Journal International*, *204*(2), 1024–1039. https://doi.org/10.1093/gji/ggv481

Korenaga, J. (2018). Crustal evolution and mantle dynamics through Earth history. *Philosophical Transactions of the Royal Society A: Mathematical, Physical and Engineering Sciences*, *376*(2132), 20170408. https://doi.org/10.1098/rsta.2017.0408

Kurz, M. D., Jenkins, W. J., & Hart, S. R. (1982). Helium isotopic systematics of oceanic islands and mantle heterogeneity. *Nature*, *297*(5861), 43–47. https://doi.org/10.1038/297043a0

Kurz, M. D., Jenkins, W. J., Schilling, J. G., & Hart, S. R. (1982). Helium isotopic variations in the mantle beneath the central North Atlantic Ocean. *Earth and Planetary Science Letters*, *58*(1), 1–14. https://doi.org/10.1016/0012-821X(82)90099-1

Labrosse, S., Hernlund, J. W., & Coltice, N. (2007). A crystallizing dense magma ocean at the base of the Earth's mantle. *Nature*, *450*(7171), 866–869. https://doi.org/10.1038/nature06355

Lenardic, A. (2018). The diversity of tectonic modes and thoughts about transitions between them. *Philosophical Transactions of the Royal Society A: Mathematical, Physical and Engineering Sciences*, *376*(2132), 20170416. https://doi.org/10.1098/rsta.2017.0416

Li, M., Black, B., Zhong, S., Manga, M., Rudolph, M. L., & Olson, P. (2016). Quantifying melt production and degassing rate at mid-ocean ridges from global mantle convection models with plate motion history. *Geochemistry, Geophysics, Geosystems*, *17*(7), 2884–2904. https://doi.org/10.1002/2016GC006439

Li, Y., Deschamps, F., Shi, Z., Guerrero, J. M., Hsieh, W.-P., Zhao, L., & Tackley, P. J. (2022). Influence of composition-dependent thermal conductivity on the long-term evolution of primordial reservoirs in Earth's lower mantle. *Earth Planets and Space*, *74*(1), 46. https://doi.org/10.1186/s40623-022-01608-3

Lourenço, D. L., Rozel, A. B., Ballmer, M. D., & Tackley, P. J. (2020). Plutonic-Squishy lid: A new global tectonic regime generated by intrusive magmatism on earth-like planets. *Geochemistry, Geophysics, Geosystems*, *21*(4), e2019GC008756. https://doi.org/10.1029/2019GC008756

Lyubetskaya, T., & Korenaga, J. (2007a). Chemical composition of Earth's primitive mantle and its variance: 1. Method and results. *Journal of Geophysical Research*, *112*(B3). https://doi.org/10.1029/2005JB004223

Lyubetskaya, T., & Korenaga, J. (2007b). Chemical composition of Earth's primitive mantle and its variance: 2. Implications for global geodynamics. *Journal of Geophysical Research*, *112*(B3). https://doi.org/10.1029/2005JB004224

MacDonald, G. J. F. (1963). The escape of helium from the Earth's atmosphere. *Reviews of Geophysics*, *1*(3), 305–349. https://doi.org/10.1029/RG001i003p00305

McDonough, W. F., & Sun, S. (1995). The composition of the Earth. *Chemical Geology*, *120*(3), 223–253. https://doi.org/10.1016/0009-2541(94)00140-4

Mukhopadhyay, S., & Parai, R. (2019). Noble gases: A record of Earth's evolution and mantle dynamics. *Annual Review of Earth and Planetary Sciences*, *47*(1), 389–419. https://doi.org/10.1146/annurev-earth-053018-060238

Müller, R. D., Flament, N., Cannon, J., Tetley, M. G., Williams, S. E., Cao, X., et al. (2022). A tectonic-rules-based mantle reference frame since 1 billion years ago—Implications for supercontinent cycles and plate–mantle system evolution. *Solid Earth*, *13*(7), 1127–1159. https://doi.org/10.5194/se-13-1127-2022

Nakagawa, T., & Tackley, P. J. (2012). Influence of magmatism on mantle cooling, surface heat flow and Urey ratio. *Earth and Planetary Science Letters*, *329–330*, 1–10. https://doi.org/10.1016/j.epsl.2012.02.011

Ono, S., Ito, E., & Katsura, T. (2001). Mineralogy of subducted basaltic crust (MORB) from 25 to 37 GPa, and chemical heterogeneity of the lower mantle. *Earth and Planetary Science Letters*, *190*(1), 57–63. https://doi.org/10.1016/S0012-821X(01)00375-2

Palin, R. M., Santosh, M., Cao, W., Li, S.-S., Hernández-Uribe, D., & Parsons, A. (2020). Secular change and the onset of plate tectonics on Earth. *Earth-Science Reviews*, *207*, 103172. https://doi.org/10.1016/j.earscirev.2020.103172

Palme, H., & O'Neill, H. S. C. (2014). 3.1—Cosmochemical estimates of mantle composition. In H. D. Holland & K. K. Turekian (Eds.), *Treatise on geochemistry* (2nd ed., pp. 1–39). Elsevier. https://doi.org/10.1016/B978-0-08-095975-7.00201-1

Panton, J., Davies, J. H., Elliott, T., Andersen, M., Porcelli, D., & Price, M. G. (2022). Investigating influences on the Pb pseudo-isochron using three-dimensional mantle convection models with a Continental reservoir. *Geochemistry, Geophysics, Geosystems*, *23*(8), e2021GC010309. https://doi.org/10.1029/2021GC010309

Panton, J., Davies, J. H., & Myhill, R. (2023). The stability of dense Oceanic crust near the core-mantle boundary. *Journal of Geophysical Research: Solid Earth*, *128*(2), e2022JB025610. https://doi.org/10.1029/2022JB025610

Phipps Morgan, J. (1998). Thermal and rare gas evolution of the mantle. *Chemical Geology*, *145*(3), 431–445. https://doi.org/10.1016/S0009-2541(97)00153-8

Porcelli, D., & Wasserburg, G. J. (1995). Mass transfer of xenon through a steady-state upper mantle. *Geochimica et Cosmochimica Acta*, *59*(10), 1991–2007. https://doi.org/10.1016/0016-7037(95)00122-0

Price, M. G., Davies, J. H., & Panton, J. (2019). Controls on the deep-water cycle within three-dimensional mantle convection models. *Geochemistry, Geophysics, Geosystems*, *20*(5), 2199–2213. https://doi.org/10.1029/2018GC008158

Récalde, N., Davies, J. H., Panton, J., Porcelli, D., & Andersen, M. (2025a). *Outputs from 3D spherical mantle convection simulations testing the influence of convection on mantle differentiation and preservation of primitive undegassed material*. NERC EDS National Geoscience Data Centre. https://doi.org/10.5285/9BCF2D04-3F29-4FF1-9089-06CB99DA7316

Récalde, N., Davies, J. H., Panton, J., Porcelli, D., & Andersen, M. (2025b). *Video files of 3D spherical mantle convection simulations testing the influence of convection on mantle differentiation and preservation of primitive undegassed material*. NERC EDS National Geoscience Data Centre. https://doi.org/10.5285/77D69231-7748-4145-A5D6-2B2A59D19CDA

Ritsema, J., Deuss, A., van Heijst, H. J., & Woodhouse, J. H. (2011). S40RTS: A degree-40 shear-velocity model for the mantle from new Rayleigh wave dispersion, teleseismic traveltime and normal-mode splitting function measurements. *Geophysical Journal International*, *184*(3), 1223–1236. https://doi.org/10.1111/j.1365-246X.2010.04884.x

Rudnick, R. L., & Gao, S. (2003). 3.01—Composition of the Continental crust. In H. D. Holland & K. K. Turekian (Eds.), *Treatise on geochemistry* (pp. 1–64). Pergamon. https://doi.org/10.1016/B0-08-043751-6/03016-4

Sammon, L. G., & McDonough, W. F. (2022). Quantifying Earth's radiogenic heat budget. *Earth and Planetary Science Letters*, *593*, 117684. https://doi.org/10.1016/j.epsl.2022.117684

Stevenson, D. J. (2003). Styles of mantle convection and their influence on planetary evolution. *Comptes Rendus Geoscience*, *335*(1), 99–111. https://doi.org/10.1016/S1631-0713(03)00009-9

Stracke, A. (2025). The geochemical concept of a "Primitive Mantle". In A. Anbar & D. Weis (Eds.), *Treatise on geochemistry* (3rd ed., pp. 1–16). Elsevier. https://doi.org/10.1016/B978-0-323-99762-1.00057-7

Stracke, A., Hofmann, A. W., & Hart, S. R. (2005). FOZO, HIMU, and the rest of the mantle zoo. *Geochemistry, Geophysics, Geosystems*, *6*(5). https://doi.org/10.1029/2004GC000824

Tackley, P. (2015). 7.12 - Mantle geochemical geodynamics. In G. Schubert (Ed.), *Treatise on geophysics* (2nd ed., pp. 521–585). Elsevier. https://doi.org/10.1016/B978-0-444-53802-4.00134-2

Tucker, J. M., van Keken, P. E., & Ballentine, C. J. (2022). Earth's missing argon paradox resolved by recycling of oceanic crust. *Nature Geoscience*, *15*(1), 85–90. https://doi.org/10.1038/s41561-021-00870-6

van der Hilst, R. D., Widiyantoro, S., & Engdahl, E. R. (1997). Evidence for deep mantle circulation from global tomography. *Nature*, *386*(6625), 578–584. https://doi.org/10.1038/386578a0

van Heck, H. J., Davies, J. H., Elliott, T., & Porcelli, D. (2016). Global-scale modelling of melting and isotopic evolution of Earth's mantle: Melting modules for TERRA. *Geoscientific Model Development*, *9*(4), 1399–1411. https://doi.org/10.5194/gmd-9-1399-2016

van Heck, H. J., & Tackley, P. J. (2008). Planforms of self-consistently generated plates in 3D spherical geometry. *Geophysical Research Letters*, *35*(19). https://doi.org/10.1029/2008GL035190

van Keken, P. E., Hauri, E. H., & Ballentine, C. J. (2002). Mantle mixing: The generation, preservation, and destruction of chemical heterogeneity. *Annual Review of Earth and Planetary Sciences*, *30*(1), 493–525. https://doi.org/10.1146/annurev.earth.30.091201.141236

Xiang, S., Huang, J., & Wu, B. (2025). Tectonic modes of mantle convection and their implications for Earth's tectonic evolution based on three-dimensional numerical simulations. *Science China Earth Sciences*, *68*(1), 270–296. https://doi.org/10.1007/s11430-024-1393-4

Xie, S., & Tackley, P. J. (2004). Evolution of U-Pb and Sm-Nd systems in numerical models of mantle convection and plate tectonics. *Journal of Geophysical Research*, *109*(B11). https://doi.org/10.1029/2004JB003176

Yang, W.-S. (1997). *Variable Viscosity Thermal Convection at Infinite Prandtl Number in a Thick Spherical Shell (unpublished doctoral dissertation)*. University of Illinois at Urbana-Champaign. Retrieved from https://hdl.handle.net/2142/86549

Yasuda, A., Fujii, T., & Kurita, K. (1994). Melting phase relations of an anhydrous mid-ocean ridge basalt from 3 to 20 GPa: Implications for the behavior of subducted oceanic crust in the mantle. *Journal of Geophysical Research*, *99*(B5), 9401–9414. https://doi.org/10.1029/93JB03205

Yuan, Q., Li, M., Desch, S. J., Ko, B., Deng, H., Garnero, E. J., et al. (2023). Moon-forming impactor as a source of Earth's basal mantle anomalies. *Nature*, *623*(7985), 95–99. https://doi.org/10.1038/s41586-023-06589-1

Zhang, X. J., Avice, G., & Parai, R. (2023). Noble gas insights into early impact delivery and volcanic outgassing to Earth's atmosphere: A limited role for the continental crust. *Earth and Planetary Science Letters*, *609*, 118083. https://doi.org/10.1016/j.epsl.2023.118083